

Cite this: *RSC Adv.*, 2016, 6, 83668Received 27th June 2016  
Accepted 11th August 2016

DOI: 10.1039/c6ra16580j

www.rsc.org/advances

# *Ab initio* and first principles theoretical investigations of triplet–triplet fluorescence in trimethylenemethane biradicals†

Yasunori Matsui,<sup>‡ab</sup> Kosuke Usui,<sup>‡c</sup> Hiroshi Ikeda<sup>ab</sup> and Stephan Irle<sup>\*cd</sup>

Theoretical studies on triplet–triplet ( $T_1 \rightarrow T_0$ ) fluorescence of the arylated trimethylenemethane (TMM) biradicals,  $^3\mathbf{2}^{**}$ , were carried out using post-Hartree–Fock *ab initio* and various first principles density functional theory methods. Analysis of optimized geometries including bond alternations and spin distributions indicates that the triplet ground ( $^3\mathbf{2}^{**}$ ) and excited ( $^3\mathbf{2}^{**}$ ) states of these biradicals have aromatic and quinoidal characteristics, respectively. Inspection of their calculated electronic structures shows that, in comparison to  $^3\mathbf{2}^{**}$ , one of the spins in  $^3\mathbf{2}^{**}$  is more delocalized onto arene-rings linked to the TMM framework.

The trimethylenemethane<sup>1</sup> (TMM, Fig. 1) biradical is a representative non-Kekulé molecule that has a triplet ground state ( $T_0$ ) owing to its  $D_{3h}$  symmetry and pair of degenerate singly-occupied molecular orbitals (SOMOs). As a result of this characteristic, many theoretical and experimental studies have been carried out probing the curious electronic structures and magnetic properties of TMM biradicals.<sup>2</sup> The fact that these biradicals emit triplet–triplet ( $T_1 \rightarrow T_0$ ) fluorescence has received great attention.<sup>3,4</sup>

In previous studies, Matsui, Ikeda, and coworkers described the observation of  $T_1 \rightarrow T_0$  fluorescence from the excited states of the 1-methyl-1-phenyl-, 1,1-diphenyl-, and 1-(2-naphthyl)-1-phenyl-substituted TMM biradicals,  $^3\mathbf{2a-c}^{**}$  (Scheme 1). For this purpose, thermoluminescence (TL)<sup>5</sup> and two-color two-laser flash photolysis measurements were conducted using the

corresponding aryl-substituted methylenecyclopropanes  $\mathbf{1a-c}$ .<sup>6</sup> Moreover,  $T_1 \rightarrow T_0$  fluorescence of these biradicals was utilized as the basis for the design of a new organic light-emitting diode, termed “organic radical light-emitting diode”.<sup>5a</sup>

The electronic configurations of the excited  $T_1$  states of the TMM biradicals are complicated by their multi-configuration character. Additionally, electronic transition wavelengths and  $T_0$  geometries of compound  $^3\mathbf{2b}$ , computed using time-dependent (TD) density functional theory (DFT)<sup>6</sup> with the B3LYP/cc-pVDZ method, are considerably different from the absorption and emission wavelengths observed experimentally.<sup>7</sup> Thus, more accurate and rigorous *ab initio* quantum chemical studies, and a detailed analysis of geometry relaxation occurring in the  $T_1$  state are required to have a greater understanding of the electronic structures of the excited states of TMM biradicals.

In the investigation described below, we carried out a theoretical study of the triplet–triplet fluorescence mechanism to accurately predict structural, electronic and  $T_1 \rightarrow T_0$  emission properties of triplet aryl-substituted trimethylenemethane biradicals  $^3\mathbf{2}^{**}$ . *Ab initio* post-Hartree–Fock methods and three

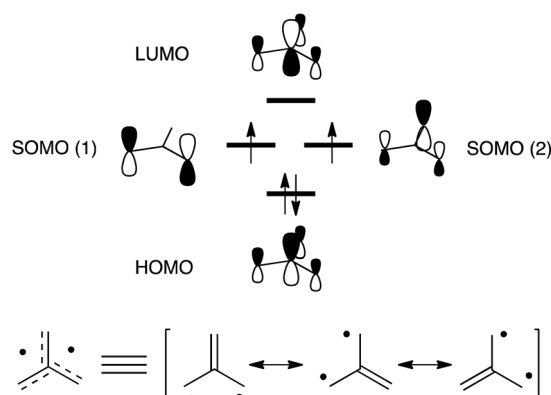


Fig. 1 (Top) Frontier molecular orbitals of the parent TMM biradical and (bottom) its corresponding Lewis resonance structures.

<sup>a</sup>Department of Applied Chemistry, Graduate School of Engineering, Osaka Prefecture University, Sakai, Osaka 599-8531, Japan

<sup>b</sup>The Research Institute for Molecular Electronic Devices (RIMED), Osaka Prefecture University, Sakai, Osaka 599-8531, Japan

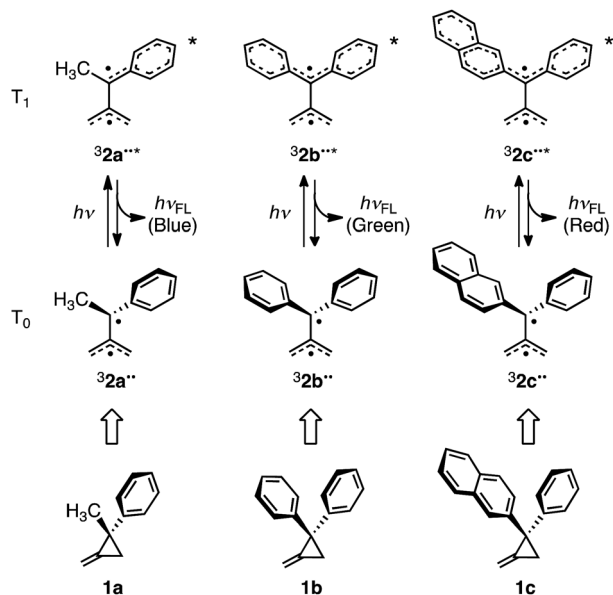
<sup>c</sup>Department of Chemistry, Graduate School of Science, Nagoya University, Nagoya, 464-8601, Japan. E-mail: sirle@chem.nagoya-u.ac.jp

<sup>d</sup>Institute of Transformative Bio-Molecules (WPI-ITbM), Nagoya University, Nagoya 464-8601, Japan

† Electronic supplementary information (ESI) available: Cartesian coordinates of all optimized structures, natural spin densities, natural charges, full citations for ref. 12 and 14. See DOI: 10.1039/c6ra16580j

‡ These authors equally contributed to this work.





Scheme 1 Chemical structures of **1a–c** and electronic structures of  $^3\mathbf{2a-c}^{**}$  and  $^3\mathbf{2a-c}^{***}$  associated with  $T_0$ – $T_1$  and  $T_1$ – $T_0$  transitions accompanying fluorescence.

different (TD-)DFT functionals were used for this purpose. When treating open-shell systems, DFT methods often suffer from spin contamination, which usually is more severe when excited rather than ground states are computed. To validate the (TD-)DFT results, high-level *ab initio* benchmark calculations were carried out on  $^3\mathbf{2}^{**}$  and the calculated spin densities and excitation energies obtained by using both types of methods were compared. In this effort, the triplet excited states of three model aryl-substituted TMM biradicals were theoretically studied because they each emit one of the three primary colors (blue, green, and red) (Scheme 1).<sup>5a</sup>

All (TD-)DFT geometry optimizations were performed using the spin-unrestricted UB3LYP, UM06-2X, and CAM-UB3LYP functionals<sup>8</sup> in conjunction with the 6-31G(d) basis set.<sup>9</sup> (TD-)DFT single point energies were obtained using the same methods, however, the larger 6-311+G(d)<sup>9c</sup> basis set was employed. For the smallest, methyl-phenyl substituted biradical,  $^3\mathbf{2a}^{**}$ , complete *ab initio* active space self-consistent field (CASSCF)<sup>10</sup> single point energy calculations with 10  $\pi$ -orbitals and 10 electrons were performed, followed by a multireference second-order Møller-Plesset perturbation (MRMP2) treatment.<sup>11</sup> All DFT calculations were conducted using Gaussian 09,<sup>12</sup> while the GAMESS-US<sup>13</sup> and MOLPRO<sup>14</sup> program packages were employed for the post-Hartree-Fock calculations. Below, we will refer to  $T_1$  and  $T_0$  states of  $\mathbf{2}^{**}$  simply as  $^3\mathbf{2}^{***}$  and  $^3\mathbf{2}^{**}$ , respectively.

In the first phase of this study, molecular geometry optimizations were carried out on  $^3\mathbf{2a-c}^{**}$  and  $^3\mathbf{2a-c}^{***}$  using various DFT functionals.<sup>15</sup> The geometries of triplet ground ( $T_0$ ) and excited ( $T_1$ ) states of these biradicals, obtained by using UB3LYP/6-31G(d), are displayed in Fig. 2, and selected bond lengths are listed in Table 1. The lengths of the C5–C6, C6–C7 and C7–C8 bonds (see Fig. 2 for atom numbering) for  $^3\mathbf{2a}^{**}$  are

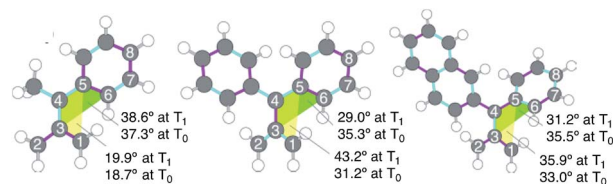


Fig. 2 Optimized structures and atom labeling of (left)  $^3\mathbf{2a-c}^{***}$ , and (center)  $^3\mathbf{2b-c}^{***}$ , and (right)  $^3\mathbf{2c-c}^{***}$ . Pink and blue bonds indicate elongated and shortened bonds of  $^3\mathbf{2-c}^{***}$  relative to  $^3\mathbf{2-c}^{**}$ .

in the range of 1.39–1.42 Å, which is typical for benzene-rings having a small degree of bond alternation. The results of applying a simulated harmonic oscillator model of the aromaticity (HOMA)<sup>16</sup> of the phenyl group in  $^3\mathbf{2a}^{**}$  (0.927) suggests that its aromaticity is relatively high (*i.e.*, roughly equal to that of benzene). In contrast, the respective C5–C6, C6–C7 and C7–C8 bond lengths in  $^3\mathbf{2a-c}^{***}$  are 1.47, 1.37, and 1.44 Å, suggesting that the degree of bond alternation is higher than in the ground state and, as a result, that the aromatic character of the phenyl group is reduced upon excitation to the  $T_1$  state. The greatly lower HOMA value (0.187) calculated for the phenyl group of  $^3\mathbf{2a-c}^{***}$  also indicates that its aromaticity is strongly reduced.

The changes in the C–C bond lengths taking place in proceeding from the diphenyl-substituted TMM biradical,  $^3\mathbf{2b}^{**}$ , to  $^3\mathbf{2b-c}^{***}$  are similar but somewhat less pronounced in comparison to those seen for the  $^3\mathbf{2a}^{**}/^3\mathbf{2a-c}^{***}$  system (Table 1). The calculated HOMA value changes are in accord with the reduction of aromaticity taking place in the phenyl group of  $^3\mathbf{2a-b}^{**}$  upon electronic excitation, with the largest change occurring in the monophenyl-substituted TMM biradical  $^3\mathbf{2a}^{**}$ . On the other hand, the calculated bond lengths and HOMA values for  $^3\mathbf{2c-c}^{***}/^3\mathbf{2c-c}^{**}$  deviate from this trend. In this case, the degree of aromaticity of the single phenyl group is less affected by excitation, presumably because excitation is localized mainly in the larger  $\pi$ -conjugated naphthyl group. The calculated dihedral angles composed of C1–C3–C4–C5 (yellow, Fig. 2) and C3–C4–C5–C6 (green) for the  $^3\mathbf{2}^{**}/^3\mathbf{2-c}^{***}$  systems also follow these trends.

An analysis of their electronic structures provides further information about the nature of the excited TMM biradicals  $^3\mathbf{2}^{***}$ . Spin distributions of  $^3\mathbf{2a-c}^{**}$  and  $^3\mathbf{2a-c}^{***}$  at Franck–

Table 1 Geometry parameters of  $^3\mathbf{2a-c}^{**}$  and  $^3\mathbf{2a-c}^{***}$  Obtained by using (TD-)UB3LYP/6-31G(d)

Biradicals	Bond lengths/Å					HOMA <sup>a</sup>
	C3–C4	C4–C5	C5–C6	C6–C7	C7–C8	
$^3\mathbf{2a}^{**}$	1.45	1.46	1.42	1.39	1.40	0.927
$^3\mathbf{2a-c}^{***}$	1.44	1.44	1.47	1.37	1.44	0.187
$^3\mathbf{2b}^{**}$	1.47	1.47	1.42	1.39	1.40	0.929
$^3\mathbf{2b-c}^{***}$	1.49	1.43	1.45	1.37	1.42	0.583
$^3\mathbf{2c}^{**}$	1.47	1.47	1.42	1.39	1.40	0.931
$^3\mathbf{2c-c}^{***}$	1.47	1.45	1.39	1.42	1.40	0.896

<sup>a</sup> Aromaticity indices of the phenyl group.



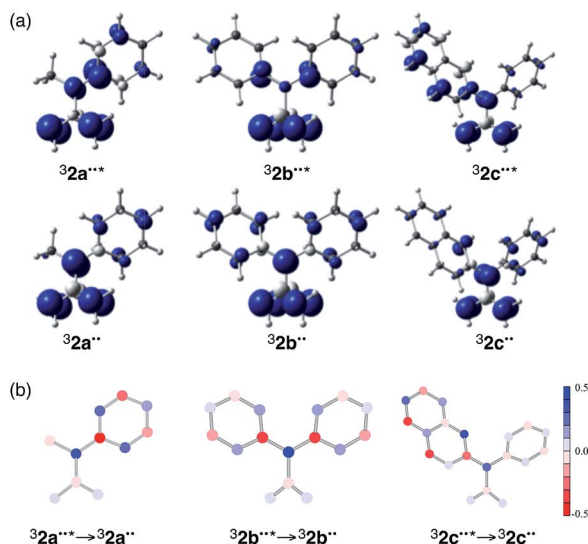


Fig. 3 (a) Spin distributions for  ${}^3\mathbf{2a-c^{**}}$  and  ${}^3\mathbf{2a-c^{**}}$  at Franck-Condon geometries. Blue and gray represent positive and negative areas of spin densities, respectively. (b)  $T_1-T_0$  difference charges occurring in the  ${}^3\mathbf{2^{**}} \rightarrow {}^3\mathbf{2^{**}}$  transitions calculated from natural orbitals for  $\alpha$ - and  $\beta$ -spin. Red and blue represent the increase and decrease of  $\alpha$ -spin density, respectively, upon excitation.

Condon geometries were determined at the (TD-)UB3LYP/6-31G\* level of theory (Fig. 3a). The results show that the spin densities of both  ${}^3\mathbf{2a^{**}}$  and  ${}^3\mathbf{2b^{**}}$  are almost completely localized at C4 (benzylic), C1 (allylic), and C2 (allylic). For  ${}^3\mathbf{2a-c^{**}}$ , the spin densities at C1 and C2 are almost identical to those of the corresponding ground state,  ${}^3\mathbf{2a-c^{**}}$ . In contrast, the spin density at C4 of  ${}^3\mathbf{2a^{**}}$  is located close to the ipso-position (C5) of the phenyl group. The change taking place in spin densities at each atom in the  ${}^3\mathbf{2b^{**}} \rightarrow {}^3\mathbf{2b^{**}}$  transition is similar to those occurring in the  ${}^3\mathbf{2a^{**}} \rightarrow {}^3\mathbf{2a^{**}}$  transition. Interestingly, the spin density changes caused by the  ${}^3\mathbf{2c^{**}} \rightarrow {}^3\mathbf{2c^{**}}$  transition occur most prominently in the 2-naphthyl group. The alterations in electronic structure are consistent with the geometrical changes that take place in all of the  ${}^3\mathbf{2^{**}} \rightarrow {}^3\mathbf{2^{**}}$  transitions (see the discussion in the previous section).

To express the spin distribution changes that take place in  ${}^3\mathbf{2^{**}} \rightarrow {}^3\mathbf{2^{**}}$  transitions in a quantitative manner, we express

the difference in the spin density of the  $i$ th atom,  $N_i^{T_1-T_0}$  by the equation given in eqn (1),

$$N_i^{T_1-T_0} = (\alpha_i^{T_1} - \beta_i^{T_1}) - (\alpha_i^{T_0} - \beta_i^{T_0}) \quad (1)$$

where  $\alpha_i^{T_1/T_0}$  and  $\beta_i^{T_1/T_0}$  are the respective natural spin densities estimated from  $\alpha$  and  $\beta$  natural orbitals for  ${}^3\mathbf{2^{**}}$  and  ${}^3\mathbf{2^{**}}$  (see Tables S7–S9†). Inspection of the data listed in Fig. 3a shows that the spin distributions at C1, C2 and C3 (the allyl moiety) do not significantly change during the  ${}^3\mathbf{2^{**}} \rightarrow {}^3\mathbf{2^{**}}$  transition. Moreover, the sum of their spin densities is approximately 1.1 each for  ${}^3\mathbf{2a-c^{**}}$  and  ${}^3\mathbf{2a-c^{**}}$  (see Table S10†). Thus, it appears that one unpaired electron is delocalized over the allyl moieties of both  ${}^3\mathbf{2a-c^{**}}$  and  ${}^3\mathbf{2a-c^{**}}$ . The other unpaired electron in the  $T_1$  excited state ( ${}^3\mathbf{2^{**}}$ ) is delocalized over the remainder of the molecule, whereas it is localized on C4 in  ${}^3\mathbf{2a-c^{**}}$ . The electronic structure change occurring upon excitation is also made apparent by inspection of the flow of spin density from C4 to C5 (Fig. 3b). The excitation-promoted, spin density reorganization decreases on proceeding from  ${}^3\mathbf{2a^{**}}$  to  ${}^3\mathbf{2c^{**}}$ . In addition, introduction of benzene or naphthalene rings leads to an enhancement in electron delocalization in the  $T_0$  state (Tables S7–S9†). The analysis presented above indicates that electronic structures of  ${}^3\mathbf{2a-c^{**}}$  and  ${}^3\mathbf{2a-c^{**}}$  can be schematically depicted in the manner shown in Scheme 1. As a result, the distribution of the second unpaired electron is controlled by introduction of aromatic groups on the TMM biradical backbone (e.g.,  ${}^3\mathbf{2c^{**}}$ ).

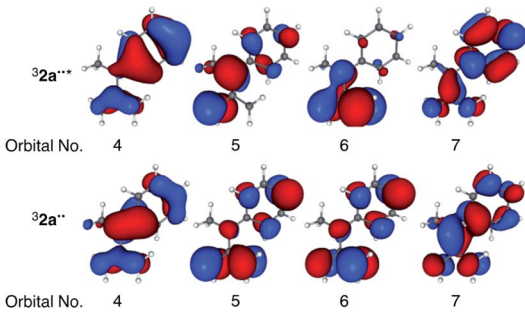
Previously, Ikeda and co-workers experimentally determined the wavelength maxima for  $T_1 \rightarrow T_0$  fluorescence of  ${}^3\mathbf{2^{**}}$  by using TL methods.<sup>5a</sup> The TL maxima of  ${}^3\mathbf{2a^{**}}$ ,  ${}^3\mathbf{2b^{**}}$  and  ${}^3\mathbf{2c^{**}}$  in methycyclohexane matrices at ca. 130 K are 451, 501, and 602 nm, respectively. In the present work, we calculated the fluorescence wavelengths of  ${}^3\mathbf{2a-c^{**}}$  using various TD-DFT functionals (Table 2). Interestingly, the fluorescence wavelengths obtained by using the UB3LYP method match well with the experimentally determined values.<sup>5</sup> Although use of the UM06-2X method also gives maxima that are close to the experimental values, it slightly overestimates the excitation energies. Utilization of the long-range corrected CAM-UB3LYP functional does not lead to improved results, suggesting that charge-transfer interactions are not important in  ${}^3\mathbf{2^{**}}$ . The use of UHF in this functional for treatment of large electronic separations suffers from a more serious spin contamination ( $\langle S^2 \rangle \sim 2.54$ – $4.01$ ), especially in the case of  ${}^3\mathbf{2c^{**}}$ .

Table 2 Fluorescence wavelength maxima ( $\lambda_{Em}$ ) and oscillator strengths ( $f$ ) of TMM biradicals obtained by experimental and various TD-DFT methods

	Exp <sup>a</sup>		TD-DFT <sup>b</sup>	
	TL	UB3LYP	UM06-2X	CAM-UB3LYP
Biradical	$\lambda_{TL}/\text{nm}$	$\lambda_{Em}/\text{nm} (\langle S^2 \rangle, f)$	$\lambda_{Em}/\text{nm} (\langle S^2 \rangle, f)$	$\lambda_{Em}/\text{nm} (\langle S^2 \rangle, f)$
${}^3\mathbf{2a^{**}}$	451	443 (2.43, 0.003)	438 (2.28, 0.005)	440 (3.10, 0.001)
${}^3\mathbf{2b^{**}}$	501	479 (2.24, 0.010)	464 (2.23, 0.018)	443 (2.54, 0.007)
${}^3\mathbf{2c^{**}}$	602	613 (2.63, 0.002)	554 (2.39, 0.004)	903 (4.01, 0.000)

<sup>a</sup> From ref. 5a. <sup>b</sup> The 6-311+G(d) and 6-31G(d) basis sets were employed for single point calculations and optimizations, respectively.



Table 3 NOON Values of  $^32a^{**}$  and  $^32a^{**}$  obtained using CASSCF(10o, 10e) calculations


NOON	Orbital no.	1	2	3	4	5	6	7	8	9	10
$^32a^{**}$		1.92	1.90	1.88	1.47	1.02	0.97	0.55	0.12	0.09	0.07
$2a^{**}$		1.96	1.92	1.90	1.87	1.00	1.00	0.13	0.10	0.08	0.04

To validate the (TD)-DFT results presented above, the electronic configuration of  $^32a^{**}$  was evaluated by employing post-Hartree-Fock CASSCF and multireference MP2 calculations. First, 10  $\pi$ -orbitals of  $^32a^{**}$  were obtained using the RHF/6-311+G(d) method for the singlet spin state. Subsequent CASSCF calculations were carried out using a full  $\pi$ -orbital (10e, 10o) active space for the triplet ground state. In Table 3 are listed the corresponding natural orbital occupation numbers (NOON), where 2, 1, and 0 indicates doubly-, singly-, and un-occupied orbitals, respectively. Importantly, a deviation of NOON from integer numbers implies that the wavefunction has multireference character.<sup>17</sup> Analysis of the NOON values for  $^32a^{**}$  indicates the existence of four doubly-occupied (NOON > 1.87), two singly-occupied (NOON  $\sim$  1.00), and four un-occupied (NOON < 0.13) orbitals within the active space. On the other hand, the NOON values of orbitals numbers 4 and 7 in  $^32a^{**}$  deviate largely from integer values, signaling that the wavefunction has multireference character. Except for natural orbitals 4–7, the NOON values and orbital shapes of  $^32a^{**}$  and  $^32a^{**}$  are almost identical. The singly-occupied natural orbital of  $^32a^{**}$  is localized on the TMM moiety, while singly occupied natural orbitals of  $^32a^{**}$  (Table 3) are delocalized on the phenyl group. The fact that this finding is consistent with the natural charge distributions obtained by using (TD)-DFT calculations (Fig. 3) validates the DFT-based results.

The CASSCF-determined emission energy of the benchmark model  $^32a^{**}$  is 2.62 eV (473 nm) and that arising from MRMP2 is 2.51 eV (495 nm). The MRMP2 result is in good agreement with that determined experimentally (2.74 eV, 451 nm), and the TD-DFT determined emission energy (2.82 eV, 440 nm) is also close to the experimental value. These findings suggest that a well-balanced use of dynamic and non-dynamic correlations is necessary for quantitatively accurate assessment of the emission wavelengths of  $^32^{**}$ . The somewhat surprising similarity of the MRMP2 and UB3LYP results show that conceptually more simple density functional approaches can be applied to the complex electronic and molecular structures of  $^32^{**}$ . This is most likely a consequence of fortuitous error compensations.

In conclusion, studies aimed at understanding the  $T_1$ - $T_0$  fluorescence of aryl-substituted TMM biradicals  $^32^{**}$  were

carried out using quantum chemical calculations. The results of calculations using high-level *ab initio* and various DFT functionals reveal that the wavefunctions of  $^32^{**}$  possesses significant multireference character. However, use of DFT approaches with sufficiently large basis sets leads to predictions of reasonable emission wavelengths of  $^32^{**}$ . In addition, the calculated changes of bond lengths and spin distributions demonstrate that significant relaxation of molecular geometries occurs in  $T_1$  on going from an aromatic ground state to quinoid structured excited state. The overall results of this work demonstrate that it is possible to use DFT-based methods to estimate accurately the fluorescence properties of organic open-shell species.<sup>18</sup> This ability should accelerate the development and application of luminescent radical materials.

## Acknowledgements

The authors acknowledge valuable discussions with Assistant Professor Daisuke Yokogawa in Nagoya University. This research was financially supported by A-STEP (No. AS231Z02594D) and ALCA (No. 1125217700) by Japan Science and Technology Agency (JST). K.U. appreciates support by the IGER program of Nagoya University. H. I. gratefully acknowledges financial support in the form of a Grant-in-Aid for Innovative Areas “ $\pi$ -Space” (No. 21108520 and 23108718 in the Area No. 2007) and “Stimuli-responsive Chemical Species” (No. 24109009 in the Area No. 2408), and the Scientific Research (B) (No. JP20044027 and JP23350023 in the Area No. 2408), and the Challenging Exploratory Research (No. JP21655016 and JP24655037) from JSPS, Japan. S. I. was partially supported by CREST grant from JST.

## Notes and references

- (a) P. Dowd, *Acc. Chem. Res.*, 1972, **5**, 242–248; (b) J. A. Berson, *Acc. Chem. Res.*, 1978, **11**, 446–453; (c) M. Abe, *Chem. Rev.*, 2013, **113**, 7011–7088.
- L. V. Slipchenko and A. I. Krylov, *J. Chem. Phys.*, 2003, **118**, 6874–6883.





- 3 (a) J. A. Berson, R. J. Bushby, J. M. McBride and M. Tremelling, *J. Am. Chem. Soc.*, 1971, **93**, 1544–1546; (b) M. S. Platz, J. M. McBride, R. D. Little, J. J. Harrison, A. Shaw, S. E. Potter and J. A. Berson, *J. Am. Chem. Soc.*, 1976, **98**, 5725–5726; (c) N. J. Turro, M. J. Mirbach, N. Harrit, J. A. Berson and M. S. Platz, *J. Am. Chem. Soc.*, 1978, **100**, 7653–7658.
- 4 H. Ikeda, H. Namai, H. Taki and T. Miyashi, *J. Org. Chem.*, 2005, **70**, 3806–3813.
- 5 (a) H. Namai, H. Ikeda, Y. Hoshi, N. Kato, Y. Morishita and K. Mizuno, *J. Am. Chem. Soc.*, 2007, **129**, 9032–9036; (b) H. Ikeda, Y. Matsui, I. Akimoto and K. Kan'no, *Aust. J. Chem.*, 2010, **63**, 1342–1347; (c) Y. Matsui, H. Namai, I. Akimoto, K. Kan'no, K. Mizuno and H. Ikeda, *Tetrahedron*, 2011, **67**, 7431–7439.
- 6 (a) P. Hohenberg and W. Kohn, *Phys. Rev.*, 1964, **136**, B864–B871; (b) W. Kohn and L. J. Sham, *Phys. Rev.*, 1965, **140**, A1133–A1138; (c) R. Bauernschmitt and R. Ahlrichs, *Chem. Phys. Lett.*, 1996, **256**, 454–464; (d) M. E. Casida, C. Jamorski, K. C. Casida and D. R. Salahub, *J. Chem. Phys.*, 1998, **108**, 4439–4449; (e) R. E. Stratmann, G. E. Scuseria and M. J. Frisch, *J. Chem. Phys.*, 1998, **109**, 8218–8224.
- 7 (a) Y. Matsui, T. Kido, E. Ohta and H. Ikeda, *Chem. Commun.*, 2014, **50**, 13963–13966; (b) Y. Matsui, D. Kawahara, E. Ohta and H. Ikeda, *Phys. Chem. Chem. Phys.*, 2013, **15**, 7064–7069.
- 8 (a) Y. Zhao and D. Truhlar, *Theor. Chem. Acc.*, 2008, **120**, 215–241; (b) C. Lee, W. Yang and R. G. Parr, *Phys. Rev. B: Condens. Matter Mater. Phys.*, 1988, **37**, 785–789; (c) A. D. Becke, *J. Chem. Phys.*, 1993, **98**, 5648–5652; (d) T. Yanai, D. P. Tew and N. C. Handy, *Chem. Phys. Lett.*, 2004, **393**, 51–57.
- 9 (a) P. C. Hariharan and J. A. Pople, *Theor. Chem. Acc.*, 1973, **28**, 213–222; (b) W. J. Hehre, R. Ditchfield and J. A. Pople, *J. Chem. Phys.*, 1972, **56**, 2257–2261; (c) R. Krishnan, J. S. Binkley, R. Seeger and J. A. Pople, *J. Chem. Phys.*, 1980, **72**, 650–654.
- 10 B. O. Roos, *Adv. Chem. Phys.*, 1987, **69**, 399–446.
- 11 (a) K. Hirao, *Chem. Phys. Lett.*, 1992, **190**, 374–380; (b) K. Hirao, *Chem. Phys. Lett.*, 1992, **196**, 397–403; (c) K. Hirao, *Chem. Phys. Lett.*, 1993, **201**, 59–66.
- 12 M. J. Frisch, *et al.*, *Gaussian 09, Revision C.01*, Gaussian, Inc., Wallingford, CT, 2009.
- 13 M. W. Schmidt, K. K. Baldridge, J. A. Boatz, S. T. Elbert, M. S. Gordon, J. J. Jensen, S. Koseki, N. Matsunaga, K. A. Nguyen, S. J. Su, T. L. Windus, M. Dupuis and J. A. Montgomery Jr, *J. Comput. Chem.*, 1993, **14**, 1347–1363.
- 14 H. J. Werner, *et al.*, *MOLPRO*, version 2010, a package of *ab initio* programs; see <http://www.molpro.net>.
- 15 For the details, see the ESI.†
- 16 HOMA is an index of aromaticity obtained by considering bond lengths of phenyl-rings. HOMA values close to 1 and 0 indicate high and low aromaticity, respectively. See: J. Kruszewskia and T. M. Krygowski, *Tetrahedron Lett.*, 1972, **13**, 3839–3842.
- 17 S. Yamanaka and K. Yamaguchi, *Bull. Chem. Soc. Jpn.*, 2004, **77**, 1269–1286.
- 18 (a) H. Namai, H. Ikeda, Y. Hoshi and K. Mizuno, *Angew. Chem., Int. Ed.*, 2007, **46**, 7396–7398; (b) Y. Hattori, T. Kusamoto and H. Nishihara, *Angew. Chem., Int. Ed.*, 2015, **54**, 3731–3734; (c) Y. Hattori, T. Kusamoto and H. Nishihara, *Angew. Chem., Int. Ed.*, 2014, **53**, 11845–11848; (d) Q. Peng, A. Obolda, M. Zhang and F. Li, *Angew. Chem., Int. Ed.*, 2015, **54**, 7091–7095.

